Final Report

On the Boundary Condition at the PCL-Mucus Interface

By Kanognudge Wuttanachamsri

05/ 2019 (finish date)

Contract No. TRG5780226

Final Report

On the Boundary Condition at the PCL-Mucus Interface

Researcher	Institute
1. Kanognudge Wuttanachamsri	King Mongkut's Institute of Technology Ladkrabang
2. Lynn Schreyer	Washington State University
3. Jack Asavanant	Advanced Virtual and Intelligent Computing (AVIC), Chulalongkorn University

Project Granted by the Thailand Research Fund
Office of the Higher Education Commission and King Mongkut's Institute of Technology Ladkrabang

Abstract

Project Code : TRG5780226

Project Title : On the Boundary Condition at the PCL-mucus Interface

Investigator : Kanognudge Wuttanachamsri

E-mail Address : whychamsri@hotmail.com

Project Period : 1 July 2014 – 30 June 2016

Abstract: ในปอดมนุษย์บนพื้นผิวของเซลล์เส้นขนที่อยู่ในเซลล์เนื้อเยื่อบุผิวในหลอดลมมีเส้นขนที่พัดโบกไปมาที่อยู่ในชั้นที่เรียกว่าเพอร์ริซิเลียรีหรือเรียกย่อ ๆ ว่าพีซีแอลและของไหลในชั้นนี้เรียกว่าของไหลพีซีแอล ซึ่งเป็นของไหลที่อัดไม่ได้ และชั้นที่อยู่เหนือชั้นพีซีแอลคือชั้นเมือก ในงานวิจัยนี้ผู้วิจัยทำการหาขอบที่เป็นอิสระที่อยู่บริเวณปลายของเส้นขนเมื่อเส้นขนทำมุมระหว่าง 40 ถึง 90 องศากับแนวราบโดยใช้วิธีการที่เรียกว่า แฟร์ (FLAIR) ซึ่งค่าที่หาได้สามารถนำไปเป็นความเร็วที่ฐานของชั้นเมือกเพื่อหาความเร็วของเมือกเพื่อช่วยในการขับเมือกออกจากร่างกายต่อไป

Keywords : สมการสโตกส์บริงแมน ของแข็งที่เคลื่อนที่ได้ ปัญหาขอบอิสระ แบบจำลองการสร้างพื้นผิวต่อประสาน

Abstract: Cilia on the surface of ciliated cells in the human lungs are organelles that beat backward and forward to generate metachronal waves. The fluid layer containing cilia coating the interior epithelial surface of the bronchi and bronchiolesis is called periciliary layer (PCL) and the fluid in this layer is named PCL fluid which is considered as an incompressible viscous fluid in this study. Above the PCL is the mucus layer. We seek for a free boundary at the tip of cilia while the cilia make an angle θ, $40^{\circ} \le \theta \le 90^{\circ}$, with the horizontal plane. The Flux Line-Segment Model for Advection and Interface Reconstruction (FLAIR) method is employed to find the shape of the free boundary based on a mixed finite element method. We use Stokes-Brinkman equations in the PCL the calculate the initial velocity of each angle θ and then apply FLAIR method to determine the free boundary at the tip of cilia so that it can be applied to be a boundary condition at the bottom of the mucus layer to be able to calculate the velocity of mucus moving out the human lungs.

Keywords : Stokes-Brinkman equations, Moving solid phase, Cilia, Free Boundary problem, Flux Line-Segment Model for Advection and Interface Reconstruction.

1. Introduction

Normal breathing with polluted particles is often unavoidable for people such as dust and bacteria. At the same time, the innate immune system in our body plays an important role to protect the body by secreting mucus from goblet cells lining beneath airway epithelium to trap the particles which are moved out of the body by the beat cycle of cilia. This system is called muco-ciliary transport studied in several literatures [1, 2, 3, 4, 5, 6, 7, 8, 9]. In the respiratory system, cilia are contained in a layer called periciliary layer (PCL) in which consists of PCL fluid. Above the PCL is a layer of viscoelastic mucus.

Figure 1 shows the respiratory system of human beginning from larynx, trachea through lungs. The cross section of the trachea is demonstrated to the left Figure 2 where the right figure is a portion of the cross section of the trachea zoomed in to get a close-up view of the surface of the trachea. In the epithelial cells, there are goblet cells ,scattered among other cells, to secrete mucus, a viscous fluid, to trap particulate matter and microorganisms preventing them from reaching the lungs. After that mucus forms a mucus blanket floating on a lower viscous fluid layer, PCL, with cilia on the surface of the epithelial cells. Cilia beat back and forth about 12 times per second to propel mucus at one millimeter per minute [10] and beat within the same plane without sweeping sideways [11]. Figure 3 illustrates the domain of interest and free boundary between the PCL and mucous layers. The arrows show the direction of cilia movement where θ is the angle between cilia and the horizontal plane. Above the mucous layer is air moving in and out of the human body. In this study, we find the shape of free boundary at the tips

of cilia so that it can be used as a boundary condition to find the velocity of mucus moving toward the throat.

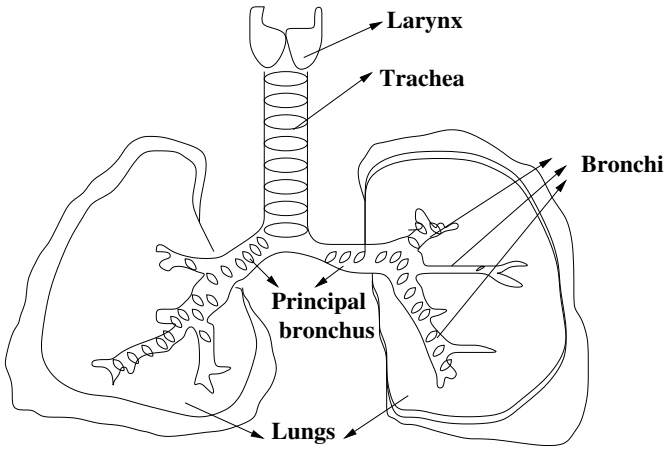

Figure 1: Anatomy of human respiratory system.

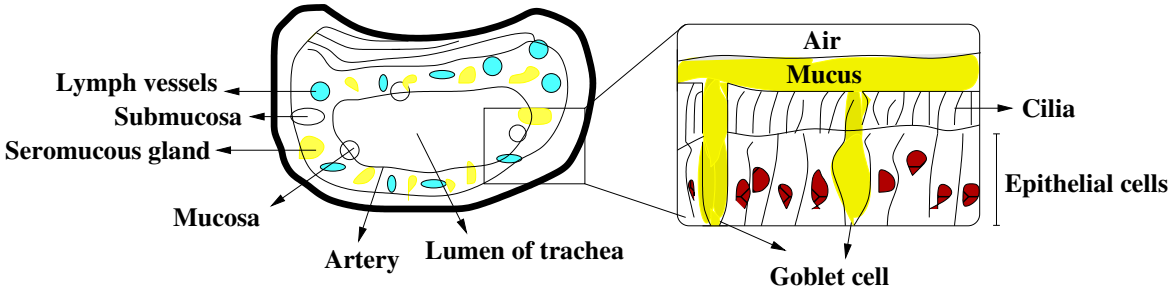

Figure 2: Patchwork of trachea at the epithelium.

Muco-ciliary clearance is fundamental and essential for the health of human respiratory system. Muco-ciliary dysfunction causes chronic airway diseases in human such as cystic fibrosis, primary ciliary dyskinesia, asthma and chronic bronchitis where the deficient mucus clearance is not completely

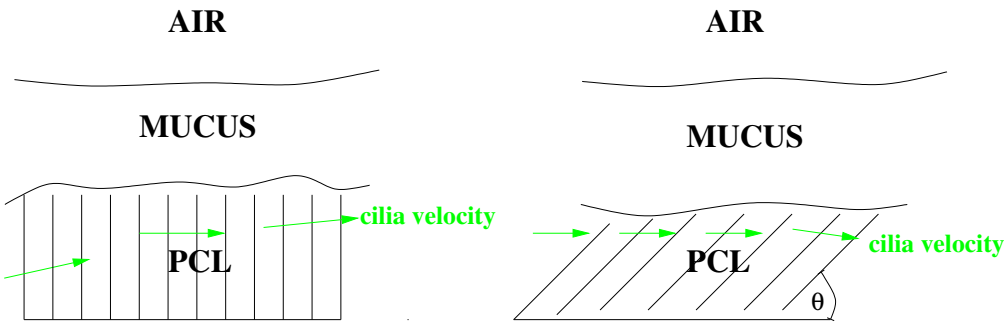

Figure 3: The cartoon picture of the movement of cilia and the free boundary at the tips of cilia.

understood. Cystic fibrosis is a disease which depletes the PCL volume and hence it is vital to investigate the effect of changing the depth of PCL and others. Therefore, the implication could be for drug manufacturers to target at finding chemicals to enhance cilia beat frequency in order to improve the muco-ciliary transport.

2. Literature review

The geometry of cilia has been studied in several articles. For instant, some considered the cilia and flagella bending properties of an axoneme [12, 13, 14]. Den Toonder and Onck [15] studied and reviewed about artificial cilia in many aspect such as Bead-spring model for artificial cilia, a superparamagnetic filament for fulid transport, modeling the interaction of active cilia with species in solution, electrostatic artificial cilia, microwalkers, artificial flagellar micro-swimmers, fluid manipulation by artificial cilia and measurement of fluid flow generated by artificial cilia.

Several literatures modeled and studied about the cilia in both experi-

mental and numerical aspects. For example, R. Quek et al. [16] simulated the ciliary flow in a three-dimensional domain using Immersed Boundary Method. They concluded that the stiffness and the cilia density effected the slip velocity. Cilia in both high and low densities have low slip velocity and the wave propagation is not supported by high stiff cilia. P. R. Sears et al. [9] used video microscopy to record ciliary motion. They converted planar ciliary motions into an empirical quantitative model, which is easy to use in examining ciliary function. If the tip of a cilium is modeled to penetrate the mucous layer, a integral equation can be used for expressing the mean velocity field in the mucous layer involving the tips of cilia [2]. Fine-tuned methods of this kind can be found in [17, 18, 19, 20].

To model the problem, since the PCL contains both PCL fluid and solid phases, cilia, it can be formed as a porous medium. When the cilia bend and make an angle θ, less than $90°$, with the horizontal plane, the region above the tips of cilia become a free-fluid layer. With slow flow in the free-fluid region, we employ Stokes equation in the domain and Brinkman equation in the porous medium for allowing the matching conditions at the interface as shown in Figure 4. The left figure illustrates only the porous medium when cilia are perpendicular to the horizontal plane and the right figure shows the cilia make an angle $\theta, \theta < 90°$, with the horizontal plane. In this study, we find the shape of the interface between the porous medium and free-fluid region.

Literatures numerically studied the fluid flow through domains using the Stokes-Brinkman equations [21, 22]. For example, Martys et al. [21] used a finite difference method to study the fluid flow near a free-fluid/porous

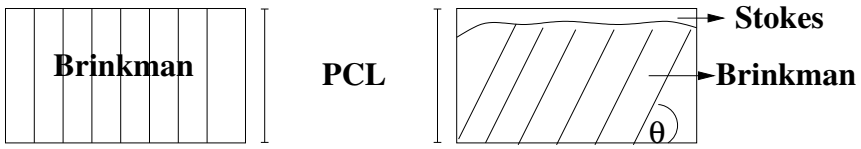

Figure 4: A porous medium and free fluid region.

medium interface in a three-dimensional domain. H. Tan and K.M.Pillai [22] employed a finite element method to solve the system of equations.

There are variety of numerical methods studying on a free boundary problem such as level-set method(LSM), Immersed Boundary Method, Simple Line Interface Calculation (SLIC), Flux Line-Segment Model for Advection and Interface Reconstruction(FLAIR) and Volume-of-Fluid method (VOF). For example, Ashgriz and Poo [23] initially developed the FLAIR method to predict the free surfaces of problems where they had the idea from Youngs [24] using a sloped line in the interface reconstruction. Hirt and Nichols [25] established the volume-of-fluid method to tract the interface. Mashayek and Ashgriz [26] claimed that the volume-of-fluid method can handle large surface deformations. Bugg and Naghashzadegan [27] compared several methods of interface tracking with different Courant numbers by predicting the motion of simple shapes. They found that increasing the grid refinement could reduce the distortion. For initially circular case, they stated that FLAIR gave the best performer. For solid body rotation, the FLAIR method was quite effective and it was preferred for all of the test cases in the literature.

Although, there are several free boundary methods, to author's knowledge, there have been no studies done on the cilia movement in the PCL with a free boundary method. In this work, we calculate the shape of the

free boundary at the tips of cilia by using FLAIR method where a mixed finite element method is employed to discretize the Stokes-Brinkman equations in a 3-dimensional domain.

3. Objectives

This research proposes to

• apply a free boundary method to track the shape of the interface at the tips of cilia using a finite element method and publish a paper with this inventive approach in a journal having impact factor indexed in ISI.

• seek for appropriate boundary conditions at the tips of cilia. These original and useful results will be published with a high impact factor in ISI.

4. Mathematical Model

In order to consider the motion of collectively cilia rather than a single cilium, the governing equation employed in this work is the Stokes-Brinkman equations in the macroscopic scale. They are upscaled by using the hybrid mixture theory (HMT) [28, 29, 30, 31] that applies the averaging theorem to average the microscale field equations to obtain the macroscale equations. The model is [32, 31]

$$\mu \mathbf{k}^{-1} \cdot (\epsilon^l \mathbf{v^l}) + \nabla p - \frac{\mu}{\epsilon^l} \Delta (\epsilon^l \mathbf{v^l}) = \rho \mathbf{g} + \mu \mathbf{k}^{-1} \cdot \epsilon^l \mathbf{v}^s + \frac{\mu}{\epsilon^l} \nabla f, \tag{1}$$

$$\nabla \cdot (\epsilon^l \mathbf{v^l}) = f, \tag{2}$$

where ϵ^l is the porosity; $\mathbf{v}^l$ and $\mathbf{v}^s$ are the velocities of the liquid and solid phases, respectively; $f = -\dot{\epsilon}^l/(1-\epsilon^l) + \nabla \cdot \epsilon^l \mathbf{v}^s$; μ is a dynamic viscosity; $\mathbf{k}^{-1}$ is

the inverse of the permeability tensor; p is pressure; $\mathbf{d}^l = 0.5(\nabla \mathbf{v}^l + (\nabla \mathbf{v}^l)^T)$ is the rate of deformation tensor; ρ is fluid density; $\mathbf{g}$ is gravity; $\dot{\epsilon}^l$ is the material time derivative of the porosity with respect to the solid phase, $\dot{\epsilon}^l = \partial \epsilon^l / \partial t + \mathbf{v}^s \cdot \nabla \epsilon^l$. Equation (1) is called Brinkman equation and without the permeability term it is the Stokes equation. Therefore equation (1) is named Stokes-Brinkman equations.

5. Model discretization

In order to find the numerical results, the discretization of the 3-dimensional Stokes-Brinkman equations is provided this section. Although the model has been discretized in [33], it is an essential detail in this study. Then, we briefly introduce them here. Define the Sobolev space

$$L_0^2(\Omega) = \{q \in L^2(\Omega) : \int_\Omega q d\Omega = 0\}. \tag{3}$$

By using a mixed finite element method, the weak formulation of the governing equation in indicial notation is to find $(\mathbf{v}, p) \in H^1(\Omega) \times L_0^2(\Omega)$ such that

$$\begin{aligned}
&\int_\Omega \mu \left[k_{ij}^{-1} v_j\right] w_i d\Omega + \frac{\mu}{\epsilon^l} \int_\Omega \left[\frac{\partial v_i}{\partial x_j} \frac{\partial w_i}{\partial x_j}\right] d\Omega - \int_\Omega p \frac{\partial w_i}{\partial x_i} d\Omega \\
&= \int_\Omega \left(\rho g_i + \mu \epsilon^l \left[k_{ij}^{-1} v_j^s\right]\right) w_i d\Omega - \frac{\mu}{\epsilon^l} \int_\Omega f \frac{\partial w_i}{\partial x_i} d\Omega - \int_\Gamma p w_i n_i d\Gamma \\
&+ \frac{\mu}{\epsilon^l} \int_\Gamma \left[\frac{\partial v_i}{\partial x_j} n_j\right] w_i d\Gamma + \frac{\mu}{\epsilon^l} \int_\Gamma f w_i n_i d\Gamma, \quad \forall\ w_i \in H_0^1(\Omega), i = 1, 2, 3,
\end{aligned} \tag{4}$$

where Ω is our computational domain; $H^1(\Omega)$ is the Hilbert space; Γ is the boundary of the domain Ω; the repeated index $j, i = 1, 2, 3$ indicates the summation but the repeat index $i, i = 1, 2, 3$ indicates the number of

equation, not the summation; $w_i \in H_0^1(\Omega)$ is the test function; $n_i, i = 1, 2, 3$ is the outward unit normal vector and gravity vector $\mathbf{g}$ is given by $\mathbf{g} = (0, 0, -g)$. Let Ω and T_h be our computational domain and a triangulation of domain Ω, respectively. Define the finite-dimensional subspaces of the Hilbert space $H^1(\Omega)$ and $L_0^2(\Omega)$ as follows

$$V_h = \{v \in H^1(\Omega) : v|_K \text{ is quadratic}, \forall K \in T_h\} \tag{5}$$

$$H_h = \{q \in L_0^2(\Omega) : q|_K \text{ is linear}, \forall K \in T_h\}. \tag{6}$$

The approximate solutions $(v_i, p) \in V_h \times H_h$ are

$$v_i(\mathbf{x}) = \sum_{m=1}^{M} \psi_m(\mathbf{x}) v_i^m = \Psi^T \mathbf{V}_i, \tag{7}$$

$$p(\mathbf{x}) = \sum_{l=1}^{L} \phi_l(\mathbf{x}) p_l = \Phi^T \mathbf{P}. \tag{8}$$

where $\mathbf{V}_i$ and $\mathbf{P}$ are vectors of the velocities and pressure, respectively; ψ_m and ϕ_l are called basis functions; Ψ and Φ are their vector forms and the integers M and L are determined by the interpolation function. For example, for a tetrahedral element, $M = 10$ for quadratic function for the velocity v_i and $L = 4$ for linear function for the pressure p. The system of equations (1)-(2) can be written in the matrix form as

$$\begin{pmatrix} \mu k_{11}^{-1}\tilde{\mathbf{A}} + \tilde{\mathbf{B}} & \mu k_{12}^{-1}\tilde{\mathbf{A}} & \mu k_{13}^{-1}\tilde{\mathbf{A}} & -\tilde{\mathbf{Q}}_1^T \\ \mu k_{21}^{-1}\tilde{\mathbf{A}} & \mu k_{22}^{-1}\tilde{\mathbf{A}} + \tilde{\mathbf{B}} & \mu k_{23}^{-1}\tilde{\mathbf{A}} & -\tilde{\mathbf{Q}}_2^T \\ \mu k_{31}^{-1}\tilde{\mathbf{A}} & \mu k_{32}^{-1}\tilde{\mathbf{A}} & \mu k_{33}^{-1}\tilde{\mathbf{A}} + \tilde{\mathbf{B}} & -\tilde{\mathbf{Q}}_3^T \\ -\tilde{\mathbf{Q}}_1 & -\tilde{\mathbf{Q}}_2 & -\tilde{\mathbf{Q}}_3 & 0 \end{pmatrix} \begin{pmatrix} \mathbf{V}_1 \\ \mathbf{V}_2 \\ \mathbf{V}_3 \\ \mathbf{P} \end{pmatrix} = \begin{pmatrix} \tilde{\mathbf{F}}_1 \\ \tilde{\mathbf{F}}_2 \\ \tilde{\mathbf{F}}_3 \\ \tilde{\mathbf{F}}_4 \end{pmatrix}, \tag{9}$$

where

$$\tilde{\mathbf{A}} = \int_{\Omega_2^e} \Psi \Psi^T d\Omega_2^e, \tag{10}$$

$$\tilde{\mathbf{K}_{ij}} = \int_{\Omega_2^e} \frac{\partial \Psi}{\partial x_i} \frac{\partial \Psi^T}{\partial x_j} d\Omega_2^e \tag{11}$$

$$\tilde{\mathbf{Q}}_i = \int_{\Omega_2^e} \Phi \frac{\partial \Psi^T}{\partial x_i} d\Omega_2^e, \tag{12}$$

$$\tilde{\mathbf{B}} = (\mu/\epsilon^l)(\tilde{\mathbf{K}_{jj}}) \tag{13}$$

$$\begin{aligned} \tilde{\mathbf{F}}_i = & \int_{\Omega_2^e} \left(-\rho g_i + \mu \epsilon^l k_{ij}^{-1} v_j^s \right) \Psi d\Omega_2^e - \frac{\mu}{\epsilon^l} \int_{\Omega_2^e} f \frac{\partial \Psi}{\partial x_i} d\Omega_2^e \\ & - \left(\int_{\Gamma_2^e} \Psi \Phi^T n_i d\Gamma_2^e \right) \mathbf{P} + \frac{\mu}{\epsilon^l} \left(\int_{\Gamma_2^e} \Psi \frac{\partial \Psi^T}{\partial x_j} n_j d\Gamma_2^e \right) \mathbf{V}_i \\ & + \frac{\mu}{\epsilon^l} \int_{\Gamma_2^e} f \Psi n_i d\Gamma_2^e, \end{aligned} \tag{14}$$

and $n_i, i = 1, 2, 3$ is the outward unit normal vector.

6. FLAIR Method

Ashgiz and Poo [23] initially introduced FLAIR method that employed the cell volume fraction to track the free surfaces and interfaces. The method is to find the line-segment orientation by considering the cell volume fractions. The sloped line segments are calculated at the boundary of every two neighboring cells. Figure 5 shows the two computational cells at the interface. The most left and right regions in blue color contain liquid and the white color is gas. The most dark blue color in the middle is the liquid transferred from donor to acceptor cells with volume V_f in one time step $\triangle t$ where u is velocity.

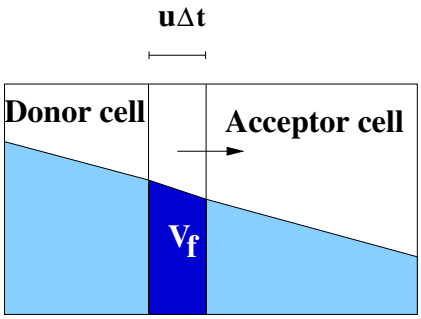

Figure 5: The volume of liquid transferred with FLAIR method.

7. Numerical Results

The velocity of each angle θ for a fixed domain is provided in [34]. In our work, to find the free surface, the initial velocity of each angle comes from the velocity of the previous angle from the fixed domain in the forward stroke. In this work, we consider the angle $\theta = 90°, 80°, ..., 40°$ where the cilia have the highest velocity at the angle $\theta = 90°$ and start for the forward stroke at this angle. Therefore the velocity of the PCL fluid at the angle $\theta = 90°$ from the fixed domain will be the initial velocity of the angle $\theta = 80°$ to find the free boundary at this angle and so on. The initial volume fraction $f_0 \in [0, 1]$ where f_0 is zero and one in an empty cell and a full cell, respectively. At a cell surface, f_0 is between zero and one. In this study, the initial f_0 is that every cell of the numerical domain lower than the tips of cilia when the cilia make angle θ with the horizontal plane has $f_0 = 1$ and $f_0 = 0$ on the other cells. Because the cilia length is nondimensionalized to be 1, when the cilia is perpendicular to the horizontal plane, $f_0 = 1$ for all cell. For the other angles, for instance, cilia make an angle θ with the horizontal plane. The hight of the layer that contains cilia is $z_0 = \xi \sin\theta$ where ξ is the cilia length

as shown in Figures 6. In this work, $\xi = 1$. From zero to z_0, the initial $f_0 = 1$ and above the z_0 value the initial $f_0 = 0$. By using FLAIR approach to track the free surfaces, the numerical results of each angle θ is illustrated in Figure 7-9. Figures 7 shows the free surfaces at the tips of cilia in PCL of the angle $\theta = 40°$ and $\theta = 50°$, from top to bottom, respectively. Similarly, the free surfaces of angles $\theta = 60°, 70°$ and $80°$ are shown in Figures 8 and 9, respectively. Because our numerical domain is a unit cube and the tips of cilia are at the top of domain when cilia is perpendicular to the horizontal plane. Therefore, the free surface for the 90 degree does not demonstrated. The free surface will be used as a free boundary at the bottom of the mucous layer to find the mucus velocity in the future work.

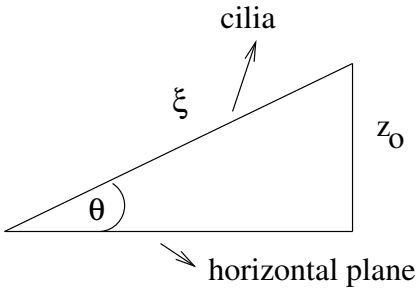

Figure 6: The angle θ between the cilia and the horizontal plane.

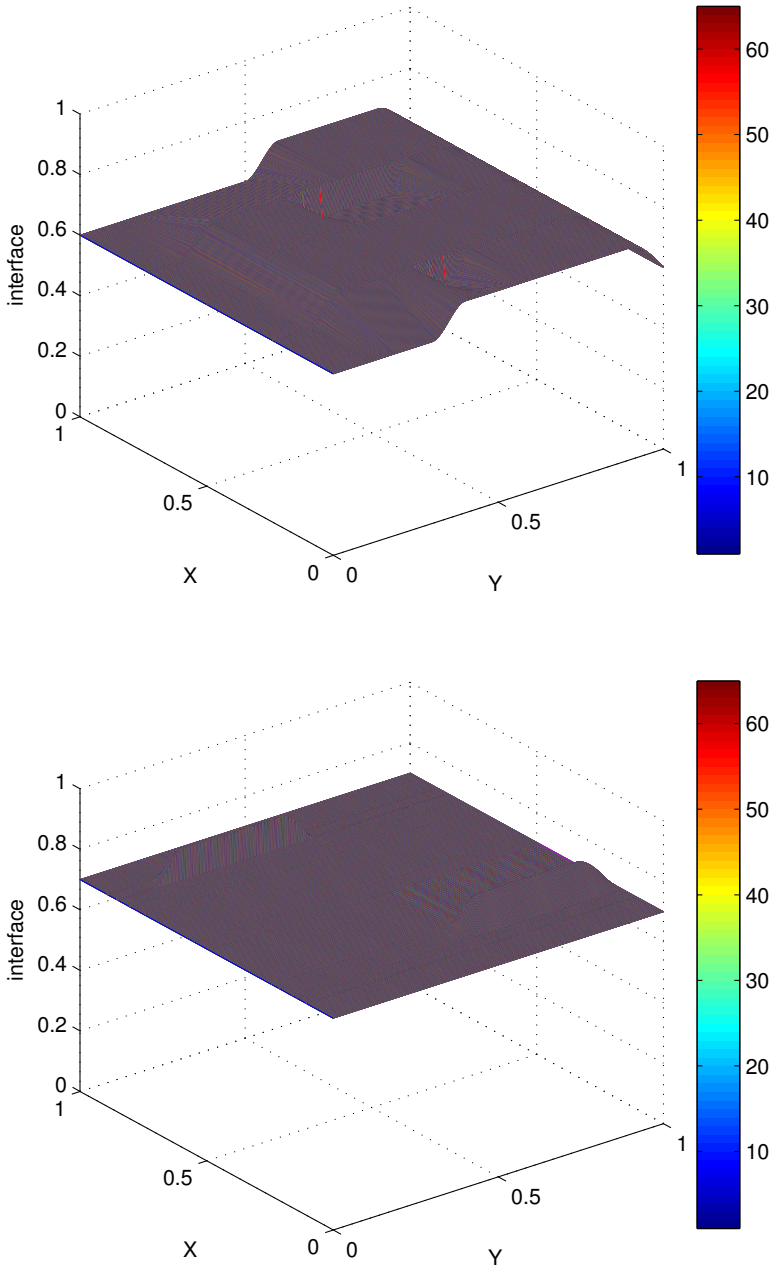

Figure 7: Free surfaces at the tips of cilia of the angle $\theta = 40°$ and $\theta = 50°$ from top to bottom.

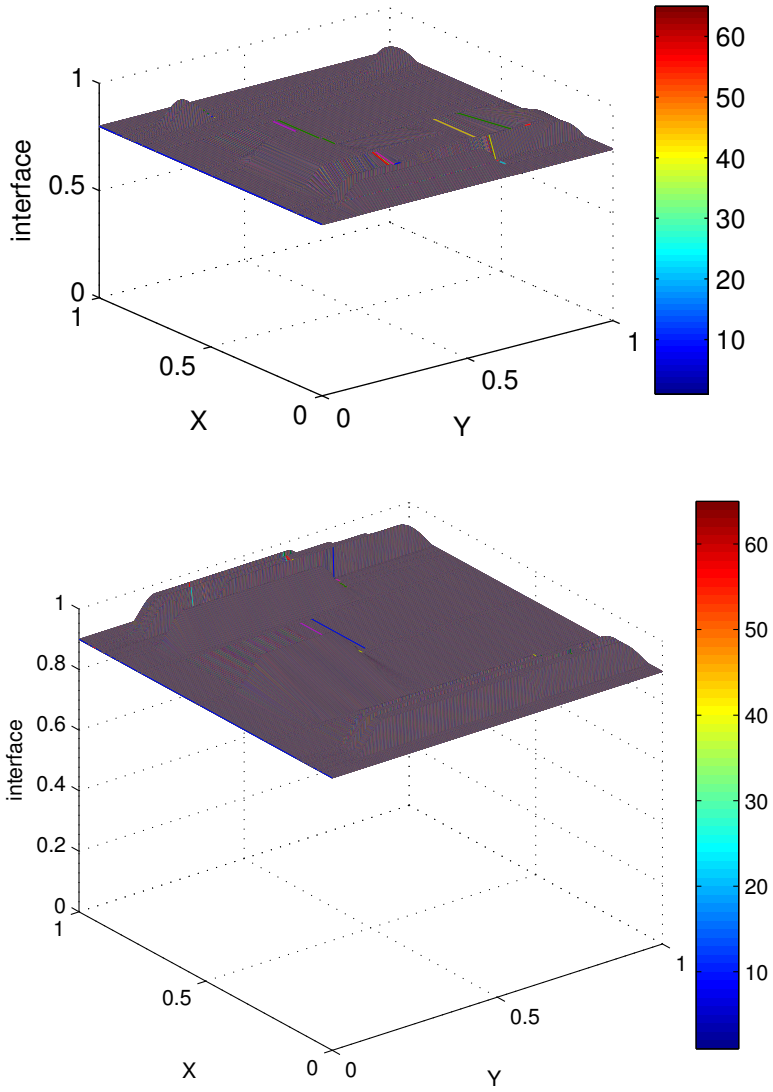

Figure 8: Free surfaces at the tips of cilia of the angle $\theta = 60°$ and $\theta = 70°$ from top to bottom.

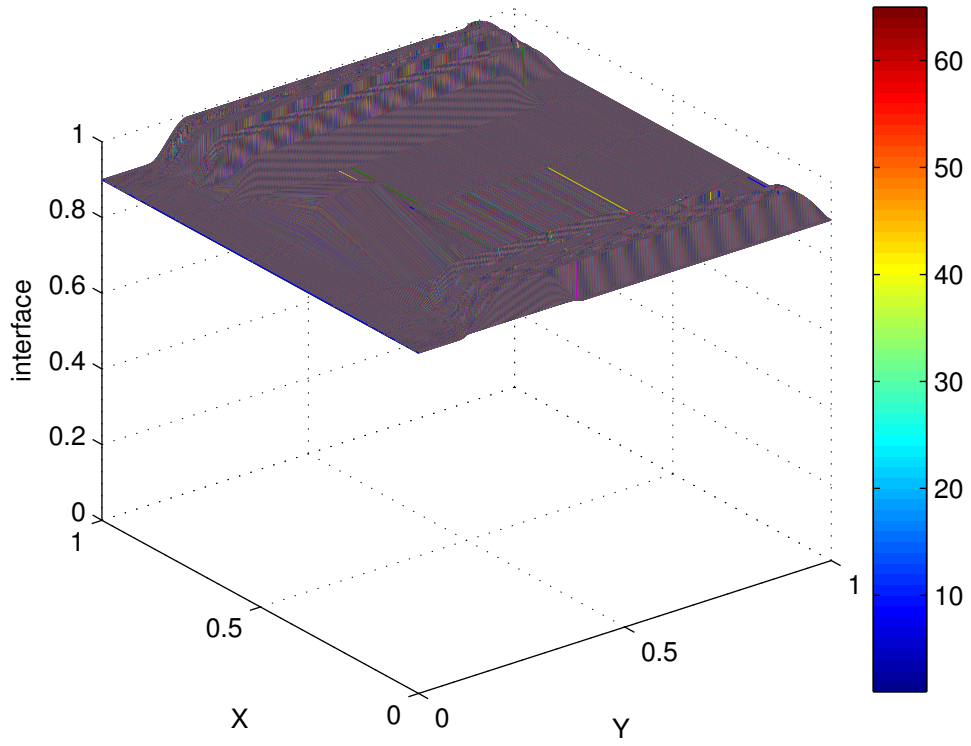

Figure 9: Free surfaces at the tips of cilia of the angle $\theta = 80°$.

8. Conclusion

We study the fluid flow due to the movement of cilia in a three dimensional domain. To expel move out of the human body, the cilia move back and forward and make and angle θ with the horizontal plane. Since the velocity of cilia affects the velocity of the PCL fluid, we use Stokes-Brinkman equations including the velocity of cilia in the external force term in the equations, which is derived by using an upscaling method named Hybrid Mixture

Theory. In this work, we focus on the forward stroke where the cilia have maximum velocity at $\theta = 90°$, which decreases to zero at $\theta = 40°$. A mixed finite element and FLAIR approaches are employed to find the numerical solutions. The velocity of the PCL fluid of each angle θ for a fixed domain is calculated in [34] by using the mixed finite element space known as the Taylor-Hood elements. We use the velocity of the fixed domain to be the initial velocity to find the free surface at the tips of cilia of each angle θ. That is the velocity of the angle $\theta = 90°$ applied to be a initial velocity of the angle $\theta = 80°$ and the process is continued to the angle $\theta = 40°$. The obtained free surfaces will be employed to be a boundary condition of the mucous layer to calculate the mucus velocity in our future work.

Reference

[1] J. R. Blake, H. Winet, On the Mechanics of muco-ciliary transport, Biorheology 17 (1980) 125–134.

[2] G. R. Fulford, J. R. Blake, Muco-ciliary Transport in the Lung, Journal of Theorectical Biology 121 (1986) 381–402.

[3] M. A. Sleigh, Adaptations of Ciliary Systems for the Propulsion of Water and Mucus, Comparative Biochemistry and Physiology 94A (1989) 359–364.

[4] W. Hofmann, B. Asgharian, Comparison of Mucociliary Clearance Velocities in Human and Rat Lungs for Extrapolation Modeling, Annals of Occupational Hygiene 46, Supplement 1 (2002) 323–325.

[5] D. J. Smith, E. A. Gaffney, J. R. Blake, A Viscoelastic Traction Layer Model of Muco-Ciliary Transport, Bulletin of Mathematical Biology 69 (2007) 289–327.

[6] D. J. Smith, E. A. Gaffney, J. R. Blake, Modelling Mucociliary Clearance, Respiratory Physiology Neurobiology 163 (2008) 178–188.

[7] P. R. Sears, W. Davis, M. Chua, K. Sheehan, Mucociliary Interactions and Mucus Dynamics in Ciliated Human Bronchial Epithelial Cell Cultures, American Journal of Physiology: Lung Cellular and Molecular Physiology 301 (2010) L181–L186.

[8] W. L. Lee, P. G. Jayathilake, Z. Tan, L. D. V., H. P. Lee, B. C.

Khoo, Muco-Ciliary Transport: Effect of Mucus Viscosity, Cilia Beat Frequency and Cilia Density, Computer & Fluids 49 (2011) 214–221.

[9] P. R. Sears, K. Thompson, M. R. Knowles, C. W. Davis, Human Airway Ciliary Dynamics, American Journal of Physiology: Lung Cellular and Molecular Physiology 304 (2012) L170–L183.

[10] W. Brawley, Health check: what you need to know about mucus and phlegm, 2014.

[11] M. Chilvers, C. O'Callaghan, Analysis of Ciliary Beat Pattern and Beat Frequency using Digital High Speed Imaging: Comparison with the Photomultiplier and Photodiode Methods, Thorax 55 (2000) 314–317.

[12] M. A. Peterson, Geometry of Ciliary Dynamics., Physical review. E, Statistical, nonlinear, and soft matter physics 80 (2009).

[13] C. B. Lindermann, A Model of Flagellar and Ciliary Functioning which Uses the Forces Transverse to the Axoneme as the Regulator of Dynein Activation, Cell Motil Cytoskeleton 29 (1994) 141–154.

[14] M. Hines, B. J. J., Three-Dimensional Mechanics of Eukaryotic Flagella, Biophysical Journal 41 (1983) 67–79.

[15] J. M. J. Den Toonder, P. R. Onck, Artificial Cilia, RSC Publishing, 2013.

[16] R. Lima, Y. Imai, T. Ishikawa, V. Cano, Visualization and Simulation of Complex Flows in Biomedical Engineering, Springer, 2014.

[17] S. Gueron, N. Liron, Ciliary Motion Modeling, and Dynamic Multicilia Interactions, Biophysical Journal 63 (1992) 1045–1058.

[18] S. Gueron, N. Liron, Simulations of 3-dimensional Ciliary Beats and Cilia Interactions, Biophysical Journal 65 (1993) 499–507.

[19] S. Gueron, K. Levit-Gurevich, Computation of the Internal Forces in Cilia: Application to Ciliary Motion, the Effects of Viscosity, and Cilia Interaction, Biophysical Journa 74 (1998) 1658–1676.

[20] S. Gueron, K. Levit-Gurevich, Energetic Considerations of Ciliary Beating and the Advantage of Metachronal Coordination, Proceedings of the National Academy of Sciences 96 (1999) 12240–12245.

[21] N. Martys, D. P. Bentz, E. J. Garboczi, Computer Simulation Study of the Effective Viscosity in Brinkman's Equation, Physics of Fluids 6 (1994) 1434–1439.

[22] H. Tan, K. M. Pillai, Finite Element Implementation of Stress-Jump and Stress-Continuity Conditions at Porous-Medium, Clear-Fluid Interface, Computers & Fluids 38 (2009) 1118–1131.

[23] N. Ashgriz, J. Poo, FLAIR: Flux Line-Segment Model for Advection and Interface Reconstruction, Journal of Computational Physics 93 (1991) 449–468.

[24] D. Youngs, Time-Dependent Multi-Material Flow with Large Distortion, Numerical Method for Fluid Dynamics (1982) 27.

[25] C. W. Hirt, B. D. Nichols, Volume of Fluid (VOF) Method for the Dynamics of Free Boundaries, Journal of Computational Physics 39 (1981) 201–225.

[26] F. Mashayek, N. Ashgriz, A Hybrid Finite?ElementÐVolume?of?Fluid Method for Simulating Free Surface Flows and Interfaces, International Journal for Numerical Methods in Fluids 20 (1995).

[27] J. Bugg, M. Naghashzadegan, Evaluation of Volume-Tracking Algorithms in Non-Straining Flows, Transactions on Modelling and Simulation 11 (1995) 83–90.

[28] L. S. Bennethum, Multiscale, Hybrid Mixture Theory for Swelling Systems with Interfaces, 2007. Note.

[29] L. S. Bennethum, J. H. Cushman, Multiphase, Hybrid Mixture Theory for Swelling Systems–I: Balance Laws, International Journal of Engineering Science 34(2) (1996) 125–145.

[30] J. H. Cushman, L. S. Bennethum, B. X. Hu, A Primer on Upscaling Tools for Porous Media, Advances in Water Resources 25 (2002) 1043–1067.

[31] T. F. Weinstein, Three-Phase Hybrid Mixture Theory for Swelling Drug Delivery Systems, Ph.D. thesis, University of Colorado Denver, 2005.

[32] K. Chamsri, Formulation of a well-posed stokes-brinkman problem with a permeability tensor, Journal of Mathematics 1 (2015) 1–7.

[33] K. Chamsri, N-dimensional stokes-brinkman equations using a mixed finite element method, Australian Journal of Basic and Applied Sciences 8 (Special 2014) 30–36.

[34] K. Wuttanachamsri, L. Schreyer, Effects of the Cilia Movement on Fluid Velocity for Fixed Domain II: Numerical Analysis, To be published (2019).

9. Output

1. K. Wuttanachamsri and L. Schreyer, On the Free Boundary Problem in Periciliary Layer, to be published, 2019.

Appendix

On the Free Boundary Problem in Periciliary Layer

Kanognudge Wuttanachamsri[1]

King Mongkut's Institute of Technology Ladkrabang, Bangkok 10520, Thailand

Lynn Schreyer[2]

Washington State University, Pullman, WA, 99164-3113

Jack Asavanant[3]

Advanced Virtual And Intelligent Computing (AVIC), Faculty of Science, Chulalongkorn University

Abstract

Cilia on the surface of ciliated cells in the human lungs are organelles that beat backward and forward to generate metachronal waves. The fluid layer containing cilia coating the interior epithelial surface of the bronchi and bronchiolesis is called periciliary layer (PCL) and the fluid in this layer is named PCL fluid which is considered as an incompressible viscous fluid in this study. Above the PCL is the mucus layer. We seek for a free boundary at the tip of cilia while the cilia make an angle $\theta, 40^\circ \leqslant \theta \leqslant 90^\circ$, with the horizontal plane. The Flux Line-Segment Model for Advection and Interface Reconstruction (FLAIR) method is employed to find the shape of the free boundary based on a mixed finite element method. We use Stokes-Brinkman

Email addresses: whychamsri@hotmail.com (Kanognudge Wuttanachamsri), Lynn.Schreyer@wsu.edu (Lynn Schreyer), jekjack@gmail.com (Jack Asavanant)

[1] *Phone number:* (666) 1282-4563

[2] *Phone number:* (509) 335-3152

[3] *Phone number:* (662) 221-3452

equations in the PCL the calculate the initial velocity of each angle θ and then apply FLAIR method to determine the free boundary at the tip of cilia so that it can be applied to be a boundary condition at the bottom of the mucus layer to be able to calculate the velocity of mucus moving out the human lungs.

Keywords: Mixed finite element method, Stokes-Brinkman equations, Moving solid phase, Cilia, Free Boundary problem, Flux Line-Segment Model for Advection and Interface Reconstruction

1. Introduction

Normal breathing with polluted particles is often unavoidable for people such as dust and bacteria. At the same time, the innate immune system in our body plays an important role to protect the body by secreting mucus from goblet cells lining beneath airway epithelium to trap the particles which are moved out of the body by the beat cycle of cilia. This system is called muco-ciliary transport studied in several literatures [1, 2, 3, 4, 5, 6, 7, 8, 9]. In the respiratory system, cilia are contained in a layer called periciliary layer (PCL) in which consists of PCL fluid. Above the PCL is a layer of viscoelastic mucus.

Figure 1 shows the respiratory system of human beginning from larynx, trachea through lungs. The cross section of the trachea is demonstrated to the left Figure 2 where the right figure is a portion of the cross section of the trachea zoomed in to get a close-up view of the surface of the trachea. In the epithelial cells, there are goblet cells ,scattered among other cells, to secrete mucus, a viscous fluid, to trap particulate matter and microorganisms

preventing them from reaching the lungs. After that mucus forms a mucus blanket floating on a lower viscous fluid layer, PCL, with cilia on the surface of the epithelial cells. Cilia beat back and forth about 12 times per second to propel mucus at one millimeter per minute [10] and beat within the same plane without sweeping sideways [11]. Figure 3 illustrates the domain of interest and free boundary between the PCL and mucous layers. The arrows show the direction of cilia movement where θ is the angle between cilia and the horizontal plane. Above the mucous layer is air moving in and out of the human body. In this study, we find the shape of free boundary at the tip of cilia so that it can be used as a boundary condition to find the velocity of mucus moving toward the throat.

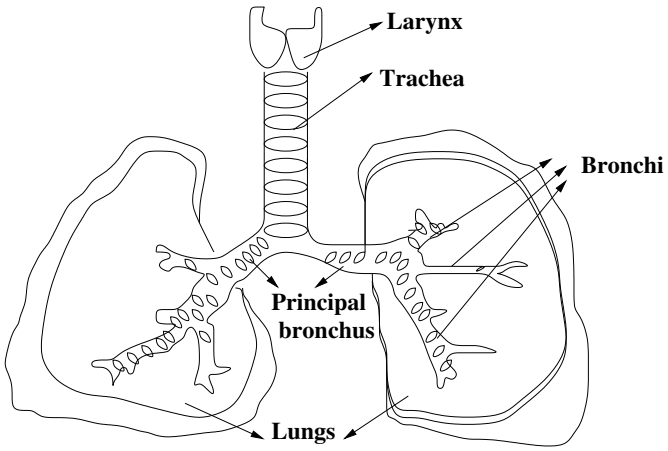

Figure 1: Anatomy of human respiratory system.

Muco-ciliary clearance is fundamental and essential for the health of human respiratory system. Muco-ciliary dysfunction causes chronic airway diseases in human such as cystic fibrosis, primary ciliary dyskinesia, asthma

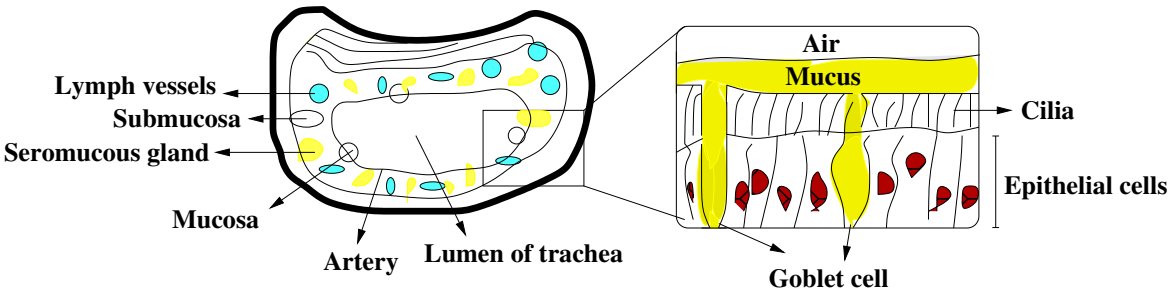

Figure 2: Patchwork of trachea at the epithelium.

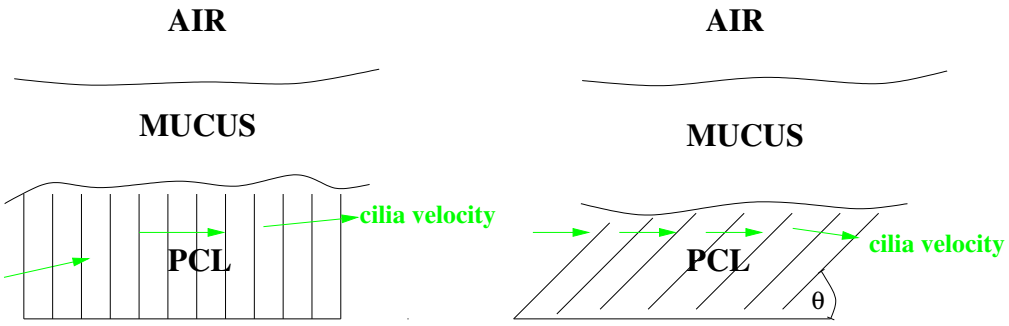

Figure 3: The cartoon picture of the movement of cilia and the free boundary at the tips of cilia.

and chronic bronchitis where the deficient mucus clearance is not completely understood. Cystic fibrosis is a disease which depletes the PCL volume and hence it is vital to investigate the effect of changing the depth of PCL and others. Therefore, the implication could be for drug manufacturers to target at finding chemicals to enhance cilia beat frequency in order to improve the muco-ciliary transport.

The geometry of cilia has been studied in several articles. For instant, some considered the cilia and flagella bending properties of an axoneme [12, 13, 14]. Den Toonder and Onck [15] studied and reviewed about ar-

tificial cilia in many aspect such as Bead-spring model for artificial cilia, a superparamagnetic filament for fulid transport, modeling the interaction of active cilia with species in solution, electrostatic artificial cilia, microwalkers, artificial flagellar micro-swimmers, fluid manipulation by artificial cilia and measurement of fluid flow generated by artificial cilia.

Several literatures modeled and studied about the cilia in both experimental and numerical aspects. For example, R. Quek et al. [16] simulated the ciliary flow in a three-dimensional domain using Immersed Boundary Method. They concluded that the stiffness and the cilia density effected the slip velocity. Cilia in both high and low densities have low slip velocity and the wave propagation is not supported by high stiff cilia. P. R. Sears et al. [9] used video microscopy to record ciliary motion. They converted planar ciliary motions into an empirical quantitative model, which is easy to use in examining ciliary function. If the tip of a cilium is modeled to penetrate the mucous layer, a integral equation can be used for expressing the mean velocity field in the mucous layer involving the tips of cilia [2]. Fine-tuned methods of this kind can be found in [17, 18, 19, 20].

To model the problem, since the PCL contains both PCL fluid and solid phases, cilia, it can be formed as a porous medium. When the cilia bend and make an angle θ, less than 90°, with the horizontal plane, the region above the tip of cilia become a free-fluid layer. With slow flow in the free-fluid region, we employ Stokes equation in the domain and Brinkman equation in the porous medium for allowing the matching conditions at the interface as shown in Figure 4. The left figure illustrates only the porous medium when cilia are perpendicular to the horizontal plane and the right figure shows the

cilia make an angle $\theta, \theta < 90°$, with the horizontal plane. In this study, we find the shape of the interface between the porous medium and free-fluid region.

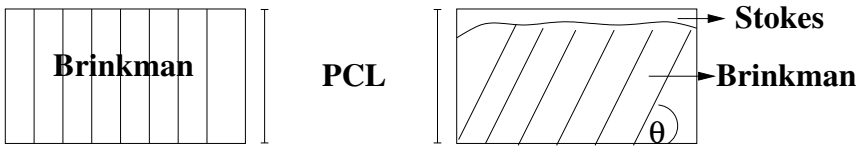

Figure 4: A porous medium and free fluid region.

Literatures numerically studied the fluid flow through domains using the Stokes-Brinkman equations [21, 22]. For example, Martys et al. [21] used a finite difference method to study the fluid flow near a free-fluid/porous medium interface in a three-dimensional domain. H. Tan and K.M.Pillai [22] employed a finite element method to solve the system of equations.

There are variety of numerical methods studying on a free boundary problem such as level-set method(LSM), Immersed Boundary Method, Simple Line Interface Calculation (SLIC), Flux Line-Segment Model for Advection and Interface Reconstruction(FLAIR) and Volume-of-Fluid method (VOF). For example, Ashgriz and Poo [23] initially developed the FLAIR method to predict the free surfaces of problems where they had the idea from Youngs [24] using a sloped line in the interface reconstruction. Hirt and Nichols [25] established the volume-of-fluid method to tract the interface. Mashayek and Ashgriz [26] claimed that the volume-of-fluid method can handle large surface deformations. Bugg and Naghashzadegan [27] compared several methods of interface tracking with different Courant numbers by predicting the motion of simple shapes. They found that increasing the grid refinement could re-

duce the distortion. For initially circular case, they stated that FLAIR gave the best performer. For solid body rotation, the FLAIR method was quite effective and it was preferred for all of the test cases in the literature.

Although, there are several free boundary methods, to author's knowledge, there have been no studies done on the cilia movement in the PCL with a free boundary method. In this work, we calculate the shape of the free boundary at the tip of cilia by using FLAIR method where a mixed finite element method is employed to discretize the Stokes-Brinkman equations in a 3-dimensional domain.

The mathematical model is stated in Section 2 and the model discretization using a mixed finite element method is given in Section 3. The FLAIR method is briefly provided in Section 5. Numerical Validation and Results is presented in Section 5 and conclusion is drawn in Section 6.

2. Mathematical Model

In order to consider the motion of collectively cilia rather than a single cilium, the governing equation employed in this work is the Stokes-Brinkman equations in the macroscopic scale. They are upscaled by using the hybrid mixture theory (HMT) [28, 29, 30, 31] that applies the averaging theorem to average the microscale field equations to obtain the macroscale equations. The model is [32, 31]

$$\mu \mathbf{k}^{-1} \cdot (\epsilon^l \mathbf{v^l}) + \nabla p - \frac{\mu}{\epsilon^l} \Delta (\epsilon^l \mathbf{v^l}) = \rho \mathbf{g} + \mu \mathbf{k}^{-1} \cdot \epsilon^l \mathbf{v}^s + \frac{\mu}{\epsilon^l} \nabla f, \tag{1}$$

$$\nabla \cdot (\epsilon^l \mathbf{v^l}) = f, \tag{2}$$

where ϵ^l is the porosity; $\mathbf{v}^l$ and $\mathbf{v}^s$ are the velocities of the liquid and solid phases, respectively; $f = -\dot{\epsilon}^l/(1-\epsilon^l)+\nabla\cdot\epsilon^l\mathbf{v}^s$; μ is a dynamic viscosity; $\mathbf{k}^{-1}$ is the inverse of the permeability tensor; p is pressure; $\mathbf{d}^l = 0.5(\nabla\mathbf{v}^l + (\nabla\mathbf{v}^l)^T)$ is the rate of deformation tensor; ρ is fluid density; $\mathbf{g}$ is gravity; $\dot{\epsilon}^l$ is the material time derivative of the porosity with respect to the solid phase, $\dot{\epsilon}^l = \partial\epsilon^l/\partial t + \mathbf{v}^s\cdot\nabla\epsilon^l$. Equation (1) is called Brinkman equation and without the permeability term it is the Stokes equation. Therefore equation (1) is named Stokes-Brinkman equations.

3. Model discretization

In order to find the numerical results, the discretization of the 3-dimensional Stokes-Brinkman equations is provided this section. Although the model has been discretized in [33], it is an essential detail in this study. Then, we briefly introduce them here. Define the Sobolev space

$$L_0^2(\Omega) = \{q \in L^2(\Omega) : \int_\Omega q d\Omega = 0\}. \tag{3}$$

By using a mixed finite element method, the weak formulation of the governing equation in indicial notation is to find $(\mathbf{v}, p) \in H^1(\Omega)\times L_0^2(\Omega)$ such that

$$\begin{aligned}
&\int_\Omega \mu\left[k_{ij}^{-1}v_j\right]w_i d\Omega + \frac{\mu}{\epsilon^l}\int_\Omega\left[\frac{\partial v_i}{\partial x_j}\frac{\partial w_i}{\partial x_j}\right]d\Omega - \int_\Omega p\frac{\partial w_i}{\partial x_i}d\Omega\\
&= \int_\Omega\left(\rho g_i + \mu\epsilon^l\left[k_{ij}^{-1}v_j^s\right]\right)w_i d\Omega - \frac{\mu}{\epsilon^l}\int_\Omega f\frac{\partial w_i}{\partial x_i}d\Omega - \int_\Gamma p w_i n_i d\Gamma\\
&+ \frac{\mu}{\epsilon^l}\int_\Gamma\left[\frac{\partial v_i}{\partial x_j}n_j\right]w_i d\Gamma + \frac{\mu}{\epsilon^l}\int_\Gamma f w_i n_i d\Gamma, \quad \forall\ w_i \in H_0^1(\Omega), i = 1,2,3,
\end{aligned} \tag{4}$$

where Ω is our computational domain; $H^1(\Omega)$ is the Hilbert space; Γ is the boundary of the domain Ω; the repeated index $j, i = 1, 2, 3$ indicates

the summation but the repeat index $i, i = 1, 2, 3$ indicates the number of equation, not the summation; $w_i \in H_0^1(\Omega)$ is the test function; $n_i, i = 1, 2, 3$ is the outward unit normal vector and gravity vector $\mathbf{g}$ is given by $\mathbf{g} = (0, 0, -g)$. Let Ω and T_h be our computational domain and a triangulation of domain Ω, respectively. Define the finite-dimensional subspaces of the Hilbert space $H^1(\Omega)$ and $L_0^2(\Omega)$ as follows

$$V_h = \{v \in H^1(\Omega) : v|_K \text{ is quadratic}, \forall K \in T_h\} \tag{5}$$

$$H_h = \{q \in L_0^2(\Omega) : q|_K \text{ is linear}, \forall K \in T_h\}. \tag{6}$$

The approximate solutions $(v_i, p) \in V_h \times H_h$ are

$$v_i(\mathbf{x}) = \sum_{m=1}^{M} \psi_m(\mathbf{x}) v_i^m = \Psi^T \mathbf{V}_i, \tag{7}$$

$$p(\mathbf{x}) = \sum_{l=1}^{L} \phi_l(\mathbf{x}) p_l = \Phi^T \mathbf{P}. \tag{8}$$

where $\mathbf{V}_i$ and $\mathbf{P}$ are vectors of the velocities and pressure, respectively; ψ_m and ϕ_l are called basis functions; Ψ and Φ are their vector forms and the integers M and L are determined by the interpolation function. For example, for a tetrahedral element, $M = 10$ for quadratic function for the velocity v_i and $L = 4$ for linear function for the pressure p. The system of equations (1)-(2) can be written in the matrix form as

$$\begin{pmatrix} \mu k_{11}^{-1}\tilde{\mathbf{A}} + \tilde{\mathbf{B}} & \mu k_{12}^{-1}\tilde{\mathbf{A}} & \mu k_{13}^{-1}\tilde{\mathbf{A}} & -\tilde{\mathbf{Q}}_1^T \\ \mu k_{21}^{-1}\tilde{\mathbf{A}} & \mu k_{22}^{-1}\tilde{\mathbf{A}} + \tilde{\mathbf{B}} & \mu k_{23}^{-1}\tilde{\mathbf{A}} & -\tilde{\mathbf{Q}}_2^T \\ \mu k_{31}^{-1}\tilde{\mathbf{A}} & \mu k_{32}^{-1}\tilde{\mathbf{A}} & \mu k_{33}^{-1}\tilde{\mathbf{A}} + \tilde{\mathbf{B}} & -\tilde{\mathbf{Q}}_3^T \\ -\tilde{\mathbf{Q}}_1 & -\tilde{\mathbf{Q}}_2 & -\tilde{\mathbf{Q}}_3 & 0 \end{pmatrix} \begin{pmatrix} \mathbf{V}_1 \\ \mathbf{V}_2 \\ \mathbf{V}_3 \\ \mathbf{P} \end{pmatrix} = \begin{pmatrix} \tilde{\mathbf{F}}_1 \\ \tilde{\mathbf{F}}_2 \\ \tilde{\mathbf{F}}_3 \\ \tilde{\mathbf{F}}_4 \end{pmatrix}, \tag{9}$$

where

$$\tilde{\mathbf{A}} = \int_{\Omega_2^e} \Psi \Psi^T d\Omega_2^e, \tag{10}$$

$$\tilde{\mathbf{K}_{ij}} = \int_{\Omega_2^e} \frac{\partial \Psi}{\partial x_i} \frac{\partial \Psi^T}{\partial x_j} d\Omega_2^e \tag{11}$$

$$\tilde{\mathbf{Q}}_i = \int_{\Omega_2^e} \Phi \frac{\partial \Psi^T}{\partial x_i} d\Omega_2^e, \tag{12}$$

$$\tilde{\mathbf{B}} = (\mu/\epsilon^l)(\tilde{\mathbf{K}_{jj}}) \tag{13}$$

$$\begin{aligned} \tilde{\mathbf{F}}_i = & \int_{\Omega_2^e} \left(-\rho g_i + \mu \epsilon^l k_{ij}^{-1} v_j^s \right) \Psi d\Omega_2^e - \frac{\mu}{\epsilon^l} \int_{\Omega_2^e} f \frac{\partial \Psi}{\partial x_i} d\Omega_2^e \\ & - \left(\int_{\Gamma_2^e} \Psi \Phi^T n_i d\Gamma_2^e \right) \mathbf{P} + \frac{\mu}{\epsilon^l} \left(\int_{\Gamma_2^e} \Psi \frac{\partial \Psi^T}{\partial x_j} n_j d\Gamma_2^e \right) \mathbf{V}_i \\ & + \frac{\mu}{\epsilon^l} \int_{\Gamma_2^e} f \Psi n_i d\Gamma_2^e, \end{aligned} \tag{14}$$

and $n_i, i = 1, 2, 3$ is the outward unit normal vector.

4. FLAIR Method

Ashgiz and Poo [23] initially introduced FLAIR method that employed the cell volume fraction to track the free surfaces and interfaces. The method is to find the line-segment orientation by considering the cell volume fractions. The sloped line segments are calculated at the boundary of every two neighboring cells. Figure 5 shows the two computational cells at the interface. The most left and right regions in blue color contain liquid and the white color is gas. The most dark blue color in the middle is the liquid transferred from donor to acceptor cells with volume V_f in one time step $\triangle t$ where u is velocity.

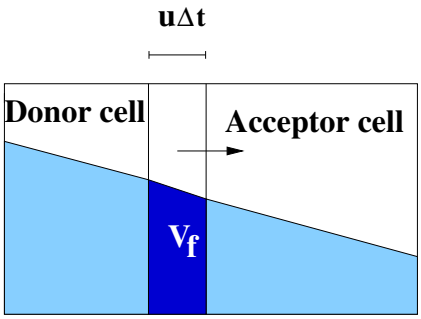

Figure 5: The volume of liquid transferred with FLAIR method.

5. Numerical Results

The velocity of each angle θ for a fixed domain is provided in [34]. In our work, to find the free surface, the initial velocity of each angle comes from the velocity of the previous angle from the fixed domain in the forward stroke. In this work, we consider the angle $\theta = 90°, 80°, ..., 40°$ where the cilia have the highest velocity at the angle $\theta = 90°$ and start for the forward stroke at this angle. Therefore the velocity of the PCL fluid at the angle $\theta = 90°$ from the fixed domain will be the initial velocity of the angle $\theta = 80°$ to find the free boundary at this angle and so on. The initial volume fraction $f_0 \in [0, 1]$ where f_0 is zero and one in an empty cell and a full cell, respectively. At a cell surface, f_0 is between zero and one. In this study, the initial f_0 is that every cell of the numerical domain lower than the tip of cilia when the cilia make angle θ with the horizontal plane has $f_0 = 1$ and $f_0 = 0$ on the other cells. Because the cilia length is nondimensionalized to be 1, when the cilia is perpendicular to the horizontal plane, $f_0 = 1$ for all cell. For the other angles, for instance, cilia make an angle θ with the horizontal plane. The hight of the layer that contains cilia is $z_0 = \xi \sin\theta$ where ξ is the cilia length

as shown in Figure 10. In this work, $\xi = 1$. From zero to z_0, the initial $f_0 = 1$ and above the z_0 value the initial $f_0 = 0$. By using FLAIR approach to track the free surfaces, the numerical results of each angle θ is illustrated in Figure 7-9. Figures 7 shows the free surfaces at the tips of cilia in PCL of the angle $\theta = 40°$ and $\theta = 50°$, from top to bottom, respectively. Similarly, the free surfaces of angles $\theta = 60°, 70°$ and $80°$ are shown in Figures 8 and 9, respectively. Because our numerical domain is a unit cube and the tips of cilia are at the top of domain when cilia is perpendicular to the horizontal plane. Therefore, the free surface for the 90 degree does not demonstrated. The free surface will be used as a free boundary at the bottom of the mucous layer to find the mucus velocity in the future work.

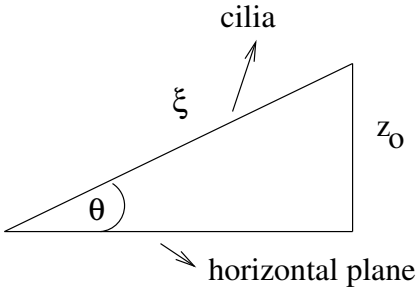

Figure 6: The angle θ between the cilia and the horizontal plane.

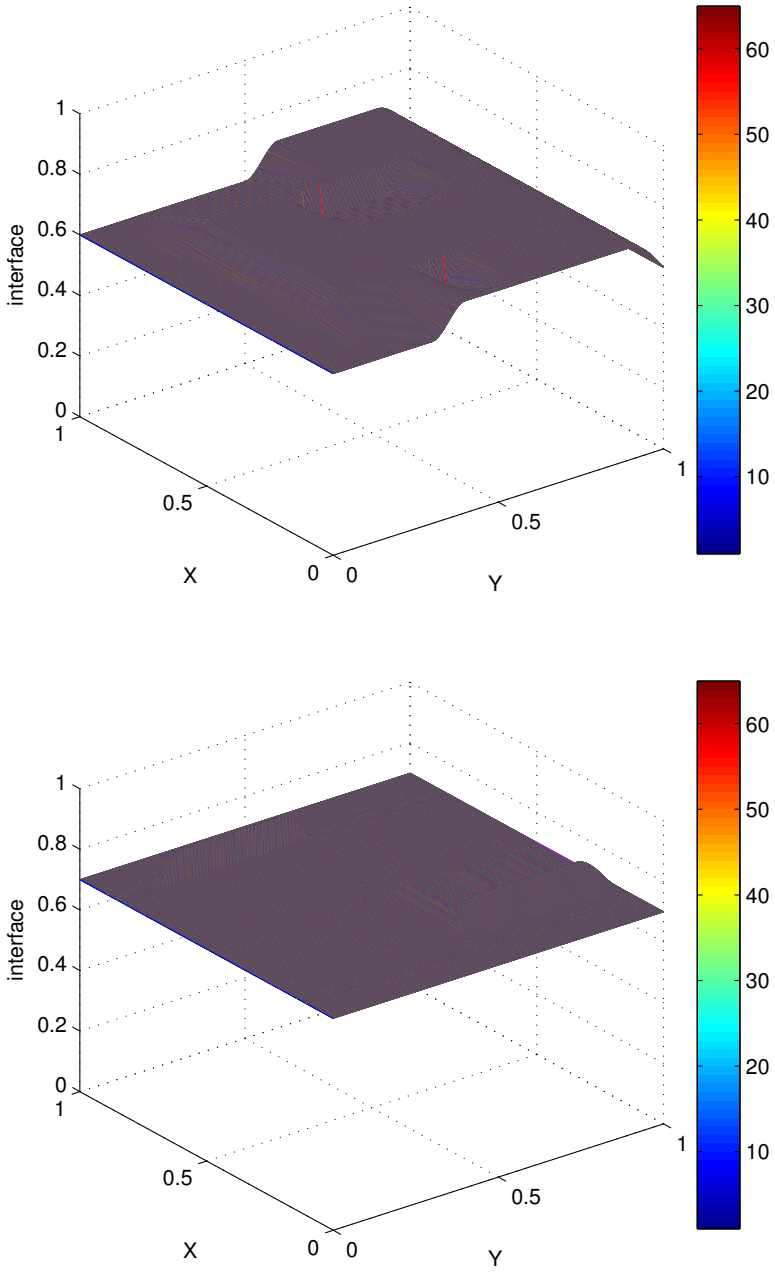

Figure 7: Free surfaces at the tips of cilia of the angle $\theta = 40°$ and $\theta = 50°$ from top to bottom.

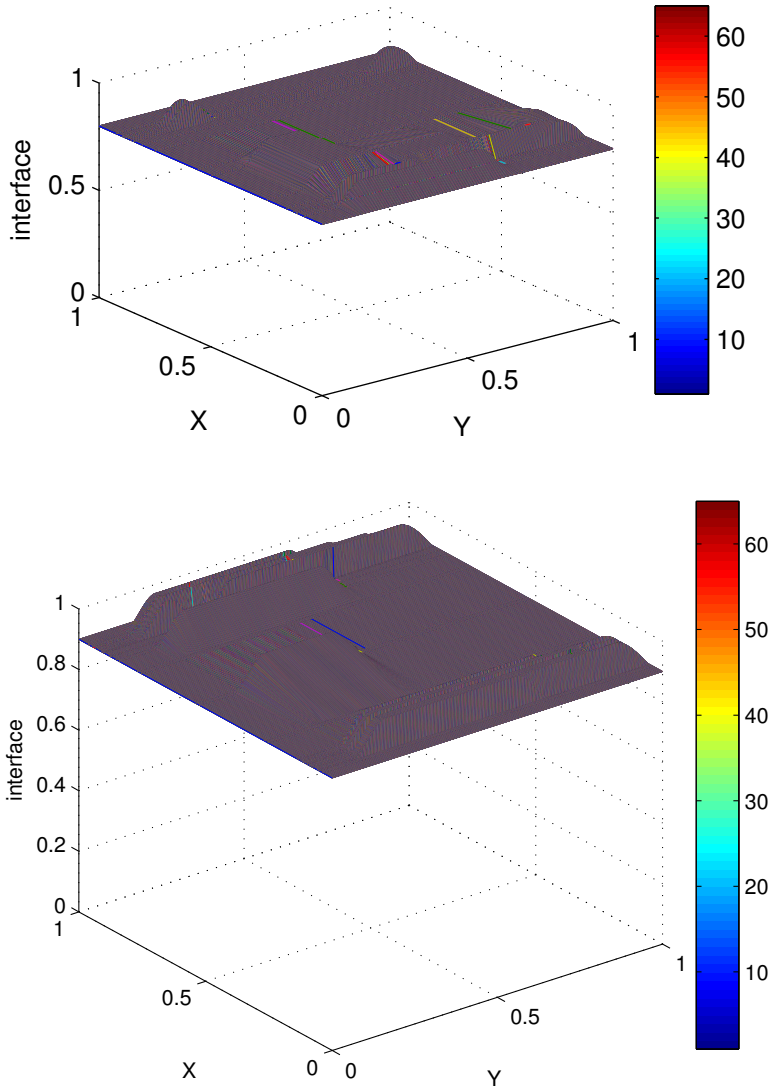

Figure 8: Free surfaces at the tips of cilia of the angle $\theta = 60°$ and $\theta = 70°$ from top to bottom.

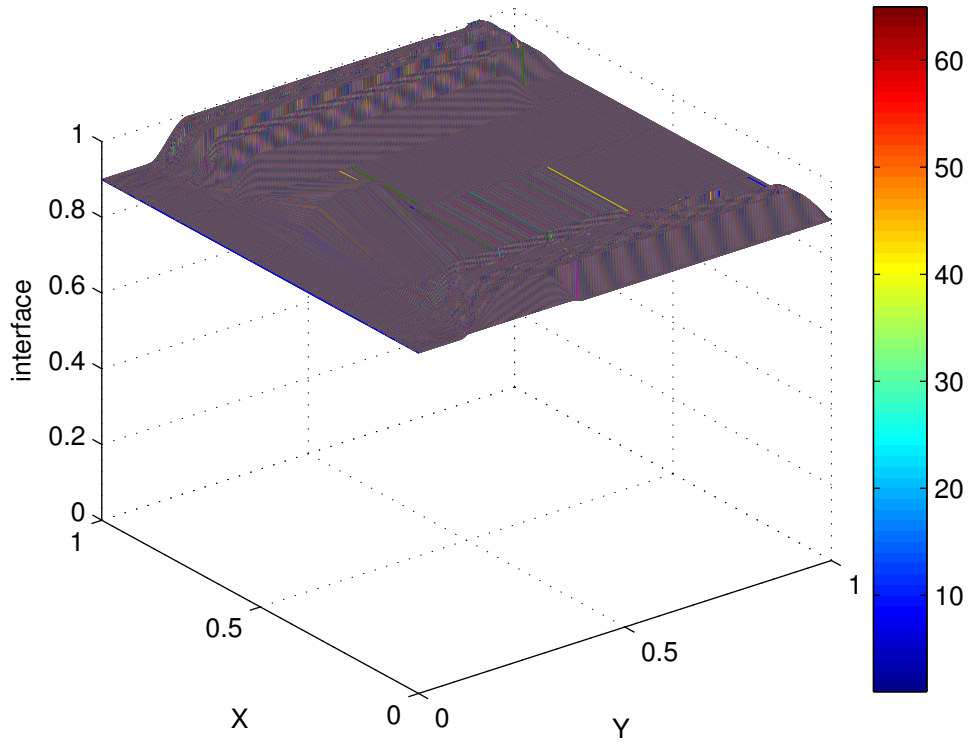

Figure 9: Free surfaces at the tips of cilia of the angle $\theta = 80°$.

6. Conclusion

We study the fluid flow due to the movement of cilia in a three dimensional domain. To expel move out of the human body, the cilia move back and forward and make and angle θ with the horizontal plane. Since the velocity of cilia affects the velocity of the PCL fluid, we use Stokes-Brinkman equations including the velocity of cilia in the external force term in the equations, which is derived by using an upscaling method named Hybrid Mixture

Theory. In this work, we focus on the forward stroke where the cilia have maximum velocity at $\theta = 90°$, which decreases to zero at $\theta = 40°$. A mixed finite element and FLAIR approaches are employed to find the numerical solutions. The velocity of the PCL fluid of each angle θ for a fixed domain is calculated in [34] by using the mixed finite element space known as the Taylor-Hood elements. We use the velocity of the fixed domain to be the initial velocity to find the free surface at the tip of cilia of each angle θ. That is the velocity of the angle $\theta = 90°$ applied to be a initial velocity of the angle $\theta = 80°$ and the process is continued to the angle $\theta = 40°$. The obtained free surfaces will be employed to be a boundary condition of the mucous layer to calculate the mucus velocity in our future work.

Acknowledgment. This research was supported by a grant from the Thailand Research Fund (TRF Fund).

[1] J. R. Blake, H. Winet, On the Mechanics of muco-ciliary transport, Biorheology 17 (1980) 125–134.

[2] G. R. Fulford, J. R. Blake, Muco-ciliary Transport in the Lung, Journal of Theorectical Biology 121 (1986) 381–402.

[3] M. A. Sleigh, Adaptations of Ciliary Systems for the Propulsion of Water and Mucus, Comparative Biochemistry and Physiology 94A (1989) 359–364.

[4] W. Hofmann, B. Asgharian, Comparison of Mucociliary Clearance Velocities in Human and Rat Lungs for Extrapolation Modeling, Annals of Occupational Hygiene 46, Supplement 1 (2002) 323–325.

[5] D. J. Smith, E. A. Gaffney, J. R. Blake, A Viscoelastic Traction Layer Model of Muco-Ciliary Transport, Bulletin of Mathematical Biology 69 (2007) 289–327.

[6] D. J. Smith, E. A. Gaffney, J. R. Blake, Modelling Mucociliary Clearance, Respiratory Physiology Neurobiology 163 (2008) 178–188.

[7] P. R. Sears, W. Davis, M. Chua, K. Sheehan, Mucociliary Interactions and Mucus Dynamics in Ciliated Human Bronchial Epithelial Cell Cultures, American Journal of Physiology: Lung Cellular and Molecular Physiology 301 (2010) L181–L186.

[8] W. L. Lee, P. G. Jayathilake, Z. Tan, L. D. V., H. P. Lee, B. C. Khoo, Muco-Ciliary Transport: Effect of Mucus Viscosity, Cilia Beat Frequency and Cilia Density, Computer & Fluids 49 (2011) 214–221.

[9] P. R. Sears, K. Thompson, M. R. Knowles, C. W. Davis, Human Airway Ciliary Dynamics, American Journal of Physiology: Lung Cellular and Molecular Physiology 304 (2012) L170–L183.

[10] W. Brawley, Health check: what you need to know about mucus and phlegm, 2014.

[11] M. Chilvers, C. O'Callaghan, Analysis of Ciliary Beat Pattern and Beat Frequency using Digital High Speed Imaging: Comparison with the Photomultiplier and Photodiode Methods, Thorax 55 (2000) 314–317.

[12] M. A. Peterson, Geometry of Ciliary Dynamics., Physical review. E, Statistical, nonlinear, and soft matter physics 80 (2009).

[13] C. B. Lindermann, A Model of Flagellar and Ciliary Functioning which Uses the Forces Transverse to the Axoneme as the Regulator of Dynein Activation, Cell Motil Cytoskeleton 29 (1994) 141–154.

[14] M. Hines, B. J. J., Three-Dimensional Mechanics of Eukaryotic Flagella, Biophysical Journal 41 (1983) 67–79.

[15] J. M. J. Den Toonder, P. R. Onck, Artificial Cilia, RSC Publishing, 2013.

[16] R. Lima, Y. Imai, T. Ishikawa, V. Cano, Visualization and Simulation of Complex Flows in Biomedical Engineering, Springer, 2014.

[17] S. Gueron, N. Liron, Ciliary Motion Modeling, and Dynamic Multicilia Interactions, Biophysical Journal 63 (1992) 1045–1058.

[18] S. Gueron, N. Liron, Simulations of 3-dimensional Ciliary Beats and Cilia Interactions, Biophysical Journal 65 (1993) 499–507.

[19] S. Gueron, K. Levit-Gurevich, Computation of the Internal Forces in Cilia: Application to Ciliary Motion, the Effects of Viscosity, and Cilia Interaction, Biophysical Journa 74 (1998) 1658–1676.

[20] S. Gueron, K. Levit-Gurevich, Energetic Considerations of Ciliary Beating and the Advantage of Metachronal Coordination, Proceedings of the National Academy of Sciences 96 (1999) 12240–12245.

[21] N. Martys, D. P. Bentz, E. J. Garboczi, Computer Simulation Study of the Effective Viscosity in Brinkman's Equation, Physics of Fluids 6 (1994) 1434–1439.

[22] H. Tan, K. M. Pillai, Finite Element Implementation of Stress-Jump and Stress-Continuity Conditions at Porous-Medium, Clear-Fluid Interface, Computers & Fluids 38 (2009) 1118–1131.

[23] N. Ashgriz, J. Poo, FLAIR: Flux Line-Segment Model for Advection and Interface Reconstruction, Journal of Computational Physics 93 (1991) 449–468.

[24] D. Youngs, Time-Dependent Multi-Material Flow with Large Distortion, Numerical Method for Fluid Dynamics (1982) 27.

[25] C. W. Hirt, B. D. Nichols, Volume of Fluid (VOF) Method for the Dynamics of Free Boundaries, Journal of Computational Physics 39 (1981) 201–225.

[26] F. Mashayek, N. Ashgriz, A Hybrid Finite?ElementÐVolume?of?Fluid Method for Simulating Free Surface Flows and Interfaces, International Journal for Numerical Methods in Fluids 20 (1995).

[27] J. Bugg, M. Naghashzadegan, Evaluation of Volume-Tracking Algorithms in Non-Straining Flows, Transactions on Modelling and Simulation 11 (1995) 83–90.

[28] L. S. Bennethum, Multiscale, Hybrid Mixture Theory for Swelling Systems with Interfaces, 2007. Note.

[29] L. S. Bennethum, J. H. Cushman, Multiphase, Hybrid Mixture Theory for Swelling Systems–I: Balance Laws, International Journal of Engineering Science 34(2) (1996) 125–145.

[30] J. H. Cushman, L. S. Bennethum, B. X. Hu, A Primer on Upscaling Tools for Porous Media, Advances in Water Resources 25 (2002) 1043–1067.

[31] T. F. Weinstein, Three-Phase Hybrid Mixture Theory for Swelling Drug Delivery Systems, Ph.D. thesis, University of Colorado Denver, 2005.

[32] K. Chamsri, Formulation of a well-posed stokes-brinkman problem with a permeability tensor, Journal of Mathematics 1 (2015) 1–7.

[33] K. Chamsri, N-dimensional stokes-brinkman equations using a mixed finite element method, Australian Journal of Basic and Applied Sciences 8 (Special 2014) 30–36.

[34] K. Wuttanachamsri, L. Schreyer, Effects of the Cilia Movement on Fluid Velocity for Fixed Domain II: Numerical Analysis, To be published (2019).